World Conference on Timber Engineering Oslo 2023

MODELLING THE EFFECT OF THREE-DIMENSIONAL GRAIN ANGLE ON THE TENSION STRENGTH OF BIRCH WOOD

Steven Collins[1], Joonas Jaaranen[2], Gerhard Fink[3]

ABSTRACT: In the present paper, the effect of three-dimensional grain direction on the tension strength of small-scale birch wood specimens is investigated. The grain angles are measured on all four surfaces of the specimens using laser light scattering technique, and afterwards, the specimens are destructively tested in tension. A numerical model is developed to predict the tensile strengths. The model is a combination of a linear elastic finite element model, with local orthotropic material orientations defined based on the measured grain orientations, and stress-based phenomenological failure criteria, with stress averaging. Strength predictions from the numerical model are compared to the experimental results, and, additionally, material strength properties are calibrated by minimizing the difference between the predictions and experimental results. A simple analytic model is further investigated and evaluated against the numerical model. Results indicate that the numerical model can predict the tensile strength of the specimens based on the measured grain angles. Stress averaging improved strength predictions by reducing localized stress peaks. Calibrated strength properties further improved the predictions and are compared with the literature. With only grain angle information, however, the numerical model does not significantly improve predictions, relative to the simple analytical model.

KEYWORDS: Grain angle, Silver birch hardwood, Tension strength, Numerical model, Finite element analysis

1 INTRODUCTION

Wood is a highly orthotropic material with much higher stiffness and strength in the longitudinal direction, compared to the transverse direction. As such, the strength of wood is dependent on fibre orientation (i.e., the grain angle), relative to the loading direction. The inclusion of grain orientation in material models may therefore improve the prediction of strength. For example, in [1], a three-dimensional (3D) material model was developed to consider the effect of knot related grain deviations on the bending strength of Scots pine. The results were validated experimentally, and the effect of knot type and knot combinations were considered in the simulation of various structural timber pieces. In another study [2], the 3D fibre direction was modelled, based on the surface grain direction obtained from laser scanning. The results indicate accurate simulations of local effects for timber boards of Norway spruce.

In previous experimental investigations on birch timber boards [3, 4], tension tests were conducted, and the tension failures often involved clear wood with grain deviations. However, methods for modelling the birch species (a diffuse porous hardwood), which consider grain orientation are lacking. Therefore, the purpose of this study was to develop and evaluate a numerical model for the prediction of tensile strength in birch small-scale clear wood specimens with known grain orientations.

2 EXPERIMENTAL INVESTIGATIONS

Data from small-scale tests specimens of silver birch wood from southern Finland was considered in this study. A total of 119 specimens were investigated. The specimens were sawn from the ends of timber boards with a wide range of grain angles [5]. The specimens are (dog-bone) shaped with a reduced gauge region of 200 mm in length (Figure 1). The radial and tangential directions of the wood are inconsistently oriented in the specimens and as such, a square cross section (w x t = 15 x 15 mm^2) was used in the reduced gauge region. The dimensions of the clamping region were l x w x t = 110 x 45 x 25 mm^3 with a 60 mm transition radius between the clamp and gauge regions. The specimens were conditioned in a climate chamber at 20ºC and 65% RH, according to international standard, ISO 13061-6 [6].

The grain angle was measured on the specimens by means of laser light scattering technique (for softwoods, termed the tracheid effect). Five laser points, spaced at 35 mm intervals, were shone on the surface, in the gauge region of the specimen, and digital images captured the elliptical reflection patterns. Figure 1a shows the laser light reflection patterns and the corresponding measurement locations. All four sides of the specimen were laser imaged. Local fibre direction is determined according to the major axis of an ellipse fit to the reflection patterns, see e.g., [7].

[1] Steven Collin, Aalto University, Department of Civil Engineering, Finland, steven.collins@aalto.fi
[2] Joonas Jaaranen, Aalto University, Department of Civil Engineering, Finland, joonas.jaaranen@aalto.fi
[3] Gerhard Fink, Aalto University, Department of Civil Engineering, Finland, gerhard.fink@aalto.fi

https://doi.org/10.52202/069179-0058

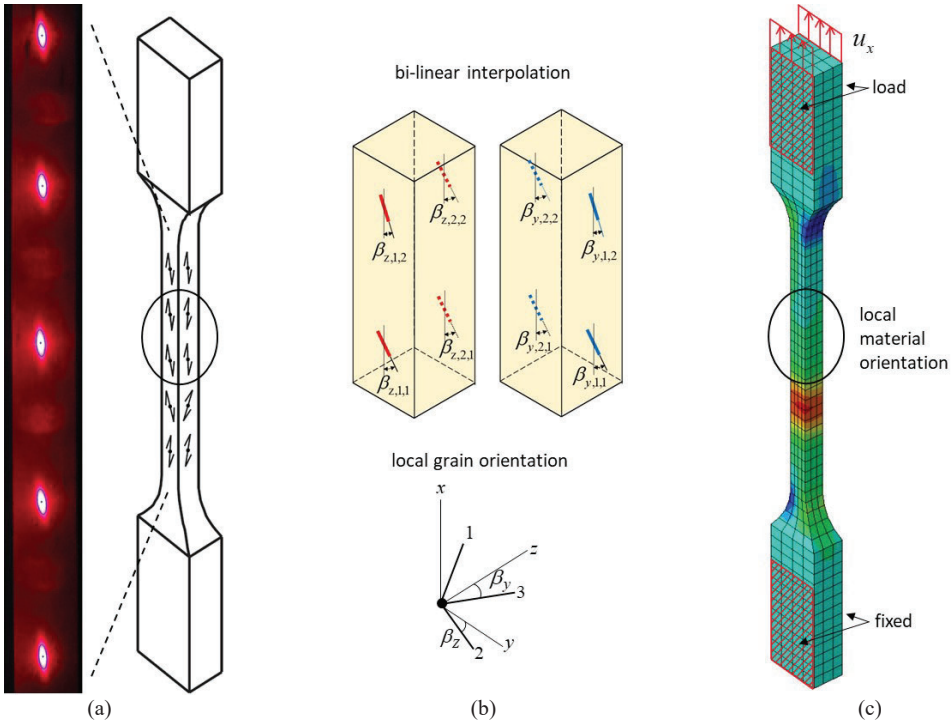

Figure 1. *(a) grain angle measurements by laser light scattering and ellipse fitting; (b) a section of the gauge region with measured grain angles, β_z and β_y used for bi-linear interpolation of the in-plane fibre direction and subsequent determination of the local grain orientation; and (c) finite element model with colour variations indicating local stresses cause by local material orientation. Boundary conditions are shown at the fixed and loaded (μ_x) ends. Element mesh size increased for illustrative purposes.*

Tension tests are subsequently conducted on the specimens using a universal testing device and the tension strength is determined according to the international standard, ISO 13061-6 [6]. The clamped area during testing was 80 x 45 mm^2. After testing, the failure mode of the specimens is analysed and documented [8].

Density was measured from a section of the gauge region after testing and the influence of density on the tension strength of this sample was investigated in a previous study [5]. Wherein, it was found that density had no unambiguous relationship with the tension strength. Therefore, density is not considered in the development of the numerical model.

3 NUMERICAL MODEL

The prediction model combines stress analysis by linear elastic finite element (FE) model with subsequent post-processing. In post processing, strength-based failure criteria with stress averaging were used to estimate the failure loads of the specimens.

3.1 STRESS ANALYSIS

The stress analyses were performed in Abaqus (Dassault Systèmes, Vélizy-Villacoublay, France) with a model of the axially loaded wood specimens, as illustrated in Figure 1c. The geometry follows nominal geometry of the actual specimens, and the model was meshed using eight-node brick elements with eight integration points (C3D8).

The mesh size was selected to have 15 x 10 elements over the specimen cross-section (note: in the figure, larger elements are used for illustration purposes). The material model was orthotropic, linear elastic, with constant properties over the whole specimen. The elastic properties were based on values for birch clear wood in [9] and are summarized in Table 1.

The grain orientations are accounted for by adjusting the local material orientations for each element. The local coordinate system is defined such that the 1-axis aligns with grain orientation and the transverse plane aligns with 23-plane.

The local orientations were determined from two grain angles, β_y and β_z (angles about the global y- and z-axes, respectively). For each element's centre point, local orientations were calculated by bilinear interpolation between the nearest measured in-plane grain angles, on opposite faces of the specimen. This is illustrated in Figure 1b. For example, the grain orientation β_z at arbitrary point (x,y,z) is obtained by interpolating between the four nearest measured grain angles $\beta_{z,i,j}$, with respect to x- and z-coordinates, while the value is constant in the y-direction. The same applies for β_y and the local grain orientation at the point is determined accordingly. Wood regions outside the limits of grain angle measurements, i.e., regions outside the gauge region, were modelled with constant grain direction according to nearest measured values.

https://doi.org/10.52202/069179-0058

Boundary conditions were applied to imitate gripping and loading in the universal testing machine. In the lower end of the specimen, all nodes on the wide faces of the gripping area are fixed in all directions. In the gripping area of the upper end of the specimen, displacement load u_x was applied in x-direction and the other directions were fixed.

For post-processing, the nodal coordinates, nodal stresses, and applied axial load F (sum nodal force in x-direction on loaded faces) were exported from each simulation. The stresses were in local coordinate systems of each node such that they can be directly used in the failure criteria. For the stresses, typical engineering notation convention is used, where σ_i are the axial stresses and τ_{ij} are the shear stresses. The indices refer to local material orientations. When referring to all the stress components at a certain point, a bold symbol $\boldsymbol{\sigma}$ is used to denote a stress vector.

Table 1: *Elastic properties in the FE model*

Property	
MOE par. to the grain E_1 [GPa]	16.3
MOE perp. to the grain $E_2 = E_3$ [GPa]	0.86
Longitudinal shear modulus $G_{12} = G_{13}$ [GPa]	1.05
Rolling shear modulus G_{23} [GPa]	0.19
Poisson's ratio $\nu_{12} = \nu_{13}$	0.46
Poisson's ratio ν_{23}	0.58

3.2 FAILURE CRITERIA

Local stresses, output from the FE model, were input into Matlab (Mathworks, Natick, Massachusetts, USA), where post-processing was performed for the prediction of tensile strength. The tensile strength was defined by most critically stressed point in the gauge region. Since there was data only for the grain orientation (longitudinal axis), but not for rotation angle of the tangential and radial axes of wood, only rotationally invariant transverse isotropic failure criteria were investigated here. Applicable criteria include Hashin criteria [10] and Tsai-Wu criterion [11]. They were originally created for composite materials but have also been widely utilised for wood. Transverse isotropic rotational invariance about 1-axis can be ensured by expressing the stress state in failure criteria in terms of following invariants [10]

$$I_1 = \sigma_1,\ I_2 = \sigma_2 + \sigma_3,\ I_3 = \tau_{23}^2 - \sigma_2\sigma_3,\quad I_4 = \tau_{12}^2 + \tau_{13}^2 \tag{1}$$

The failure criteria were based on the uniaxial strengths, namely, tensile strength parallel to the grain $f_{t,0}$, compressive strength parallel to the grain $f_{c,0}$, tensile strength perpendicular to the grain $f_{t,90}$, compressive strength perpendicular to the grain $f_{c,90}$, longitudinal shear strength f_v and rolling shear strength f_r.

The Hashin failure criterion [10] consist of four separate criteria, two for tensile modes and two for compressive modes. In this study, only the tensile failure modes were considered. The first mode (Equation 2) is "fibre tension" mode, which corresponds to failure parallel to the grain. The second mode (Equation 3) is "matrix tension" mode, which corresponds to failure perpendicular to the grain. In the equations, $\langle\ \rangle$ are Macaulay brackets denoting that $\langle x\rangle = x$ if $x > 0$, and $\langle x\rangle = 0$ otherwise.

$$\left(\frac{\langle\sigma_1\rangle}{f_{t,0}}\right)^2 + \frac{\tau_{12}^2 + \tau_{23}^2}{f_v^2} = 1 \tag{2}$$

$$\left(\frac{\langle\sigma_2 + \sigma_3\rangle}{f_{t,90}}\right)^2 + \frac{\tau_{23}^2 - \sigma_2\sigma_3}{f_r^2} + \frac{\tau_{12}^2 + \tau_{23}^2}{f_v^2} = 1 \tag{3}$$

Tsai-Wu [11] failure criterion consists of a single ellipsoidal failure surface in the stress space. Its transverse isotropic form is

$$\begin{aligned} &F_1\sigma_1 + F_2(\sigma_2 + \sigma_3) \\ &+F_{11}\sigma_1^2 + 2F_{12}\sigma_1(\sigma_2 + \sigma_3) + F_{22}(\sigma_2 + \sigma_3)^2 \\ &+F_{44}(\tau_{23}^2 - \sigma_2\sigma_3) + F_{55}(\tau_{12}^2 + \tau_{23}^2) = 1 \end{aligned} \tag{4}$$

in which F_i and F_{ij} are the strength parameters. They are defined in terms of uniaxial strengths as

$$\begin{aligned} F_1 = \frac{1}{f_{t,0}} - \frac{1}{f_{c,0}}, F_2 = \frac{1}{f_{t,90}} - \frac{1}{f_{c,90}}, \\ F_{11} = \frac{1}{f_{t,0}f_{c,0}}, F_{22} = \frac{1}{f_{t,90}f_{c,90}}, \\ F_{44} = \frac{1}{f_r^2}, F_{55} = \frac{1}{f_v^2} \end{aligned} \tag{5}$$

Parameter F_{12} (in Equation 4) is an off-axis strength parameter that, according to Tsai and Wu [11], should be determined based on off-axis tests. There exist also various approaches to estimate it from the other strength properties in the literature. However, in the present study, the criterion was simplified by setting $F_{12} = 0$.

3.3 STRESS AVERAGING

Purely stress-based strength predictions, without modelling related hardening or softening behaviour, assume a perfectly brittle material behaviour. However, stress-based criteria have been utilised also for quasi-brittle materials by stress averaging method [12, 13], which was also investigated in this study. Here, the averaging length was not derived from fracture mechanics since unambiguous fracture properties were not available, and the existing method for estimating the averaging length has been derived only for plane stress cases.

In the averaging approach adopted, the local stresses $\boldsymbol{\sigma}$ were replaced with average stresses $\overline{\boldsymbol{\sigma}}$ in the failure criteria (Equations 2-4). In this study, the same averaging is applied to all stress components. Averaged stresses at node k are computed by

$$\overline{\boldsymbol{\sigma}}_k = \frac{\sum_{p=1}^{N} w_{kp}\boldsymbol{\sigma}_p}{\sum_{p=1}^{N} w_{kp}} \tag{5}$$

where w_{kp} and $\boldsymbol{\sigma}_p$ are the weight and the stresses at point p. The weights are calculated with a Gaussian smoothing function, based on Euclidian distances d_{kp} between points k and p, as

$$w_{kp} = \exp\left(-\frac{d_{kp}^2}{l_c^2}\right) \quad (6)$$

where l_c is a length scale parameter. The length scale parameter is a distance after which the local stresses have relatively small contribution to the averaged stresses. The relation between the weight function and l_c is shown in Figure 2.

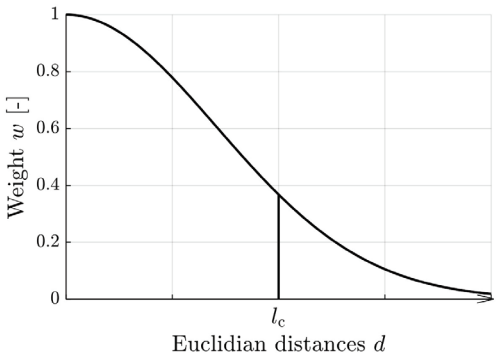

Figure 2: *Stress averaging weight factor w, as a function of Euclidian distance d to the surrounding FE nodes.*

3.4 ULTIMATE LOAD PREDICTION

Prediction of ultimate load was based on utilization ratio in the failure criteria and load F from the FE model. The utilization for point k was defined by the failure function in Equation (7), where $\bar{\boldsymbol{\sigma}}_{\boldsymbol{k}}$ is the averaged stress state at point k. Assuming proportional stresses, the ratio between failure stresses and applied stresses, g_k, was obtained by solving Equation (8). Furthermore, assuming linear elasticity, the ratio between ultimate load and applied load is equal to minimum g_k, and thus, the predicted failure load F_u can be estimated by Equation (9). Coordinates of the point with min(g_k) also give the estimated failure location.

$$f_k = f(\bar{\boldsymbol{\sigma}}_{\boldsymbol{k}}) \quad (7)$$

$$f_k(g_k \bar{\boldsymbol{\sigma}}_{\boldsymbol{k}}) = 1 \quad (8)$$

$$F_u = \min_{k=1\ldots N}(g_k)\, F \quad (9)$$

4 RESULTS

4.1 EXPERIMENTAL DATA

The failure modes were visually inspected and classified according to the five classes shown in Figure 3. A wide range of tension strength values, and grain angles are observed from the experimental investigations. Figure 4 shows the relationship between tension strength and the maximum 3D grain angle measured on the specimens. The grain angle has a clear influence on the strength. In most cases, the failure occurred within the gauge region of the specimens, however, specimens with splintering and longitudinal shear type failures (circle symbols) often had fractures that extend outside the gauge region and into the clamping zone. These specimens have greater scatter and present challenges for strength predictions.

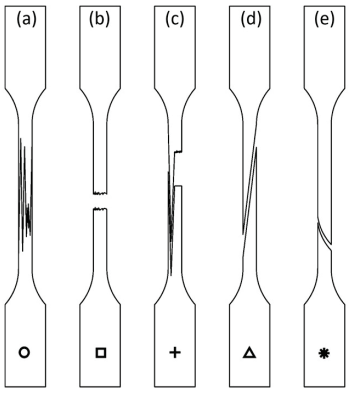

Figure 3. *Typical experimental failure modes used for classification: splintering/longitudinal shear (a), tension (b), combined tension & shear (c), sloping shear (d), and local (curved) grain deviation (e).*

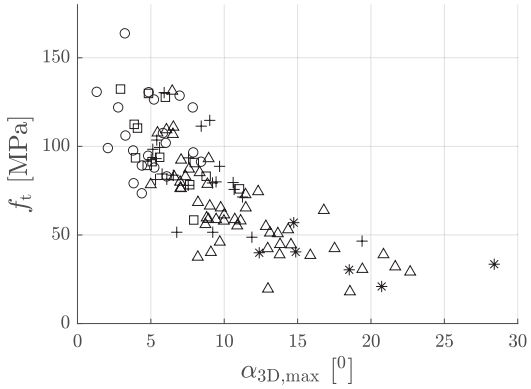

Figure 4: *Comparison between tension strength and measured maximum 3D grain angle.*

4.2 NUMERICAL MODEL

Figure 5 shows comparisons between the tensile strengths from the experimental tests and the predicted strengths according to the numerical models. The results are illustrated for the Hashin and Tsai-Wu failure criteria.

In all cases, stress averaging is applied, whereby the stress values obtained from FE analysis are effectively smoothed, i.e., the peak values are reduced, and the predicted strength values generally increase. Without stress averaging, the predicted strengths, using the initial strength values from literature (Table 2), are significantly underestimated, particularly for specimens of higher strengths. A range of l_c values (from 5 to 15 mm) were investigated and l_c = 5 mm was selected as it improves the initial results, i.e., the fit between predicted and experimental strengths. Nonetheless, l_c values up to 10 mm provide similar improvements. According to literature [14], averaging lengths from 4 mm to 20 mm are typical.

https://doi.org/10.52202/069179-0058

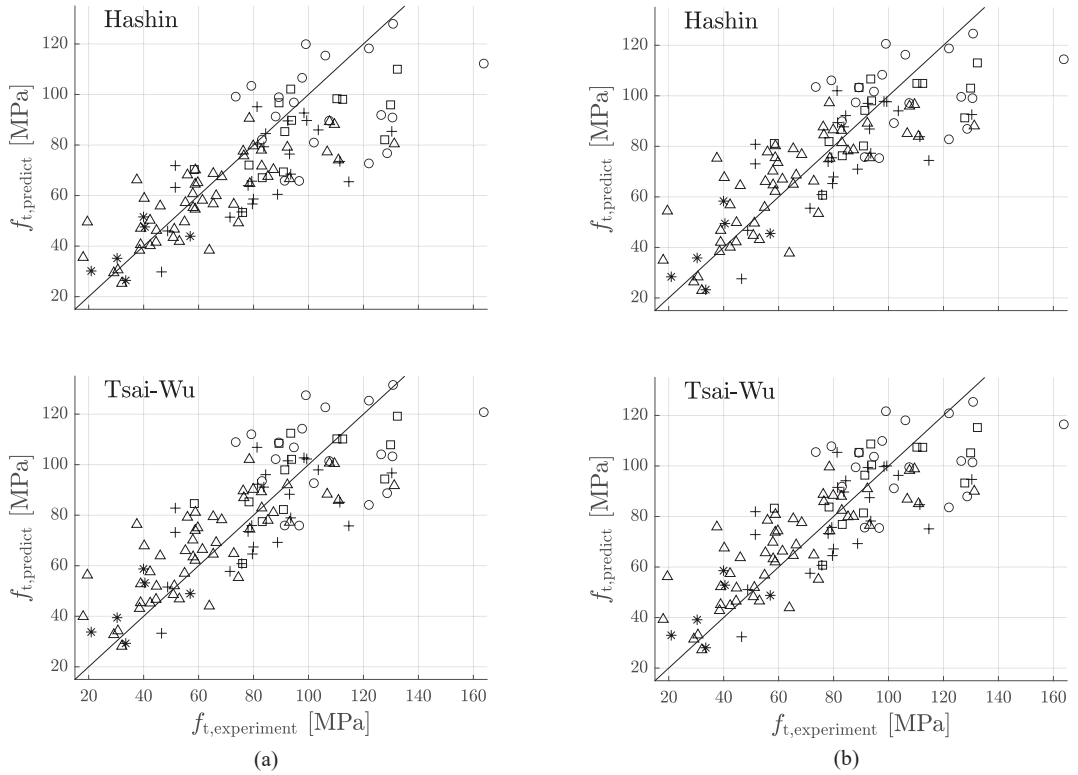

Figure 5. *Comparison between predicted and experimental strength for the Hashin and Tsai-Wu failure criteria when applying (a) strength values from literature, (b) calibrated strength values (calibrated to the whole sample). Stress averaging with l_c = 5 mm is applied in all cases.*

Table 2: *Initial and calibrated strength parameters. References for the initial parameters are shown next the values.*

	Initial	Hashin		Tsai-Wu		Hankinson	
	(uncalibrated)	Whole sample	Gauge	Whole sample	Gauge	Whole sample	Gauge
$f_{t,0}$ [MPa]	137 [15]	130	150	130	140	127	143
$f_{c,0}$ [MPa]	53 [16]	-	-	56	55	-	-
$f_{t,90}$ [MPa]	7.0 [15]	4.4	7.3	6.0	6.6	6.17	8.61
$f_{c,90}$ [MPa]	6.5 [16]	-	-	6.2	6.6	-	-
f_v [MPa]	12 [15]	15	13	13	12	-	-
f_r [MPa]	3.5 [17]	3.3	*	4.2	3.8	-	-
n	-	-	-	-	-	1.79	1.50

*Unstable parameter

Figure 5a illustrates the comparison when the strength properties from literature are considered. It is observed that the Hashin criterion underestimates specimens with higher strengths, yet the Tsai-Wu criterion has a minor bias towards overestimation of strength for the lower strengths and some underestimation for the highest strengths. Since the literature values (of which are generally lacking for silver birch) are from different source materials (excluding the compression strengths, they are determined from the same sample material), the literature values applied may not be ideal for the present sample.

An additional feature captured in the numerical model is the stress concentrations that develop around the curved tapering region of the dog-bone shaped specimen. This leads to predicted failures occurring more frequently in the ends of the gauge region, compared to the inner regions, and this behaviour is also exhibited experimentally.

Investigations into strength properties that are calibrated to the experimental results are conducted. Calibrated strength values are determined by simultaneously optimizing all uniaxial strength properties included in the failure criteria, by minimizing the sum of the squared residuals between

the predicted and experimental strengths. Stress averaging with l_c = 5 mm is maintained. Calibration is performed on both the whole sample and only on specimens that have failed within the gauge region (gauge specimens). Specimens with splintering or longitudinal shear type failure are predominantly those which have failures extending outside the gauge region. Effects from the test setup for specimens with failures extending into clamped region is not captured in the model and may have higher strengths, compared to the model predictions.

The strength properties after calibration are given in Table 2 and Figure 5b illustrates the comparison between experimental and predicted results, according to the calibrated strength properties for the whole sample. The calibrated strengths generally agree with the values from literature, although some considerable differences are obtained. The tension strengths (parallel and perpendicular to grain) calibrated to the whole sample are notably lower than the literature values, especially for Hashin. Calibrations with the gauge specimens and Tsai-Wu criteria largely concur with the literature values. For Hashin, calibrations with the gauge specimens provide similar values to literature except the tension strength parallel to the grain is, in this case, rather high.

Overall, the error when applying calibrated predictions (whether the whole sample or the gauge specimens are considered) is only slightly lower compared to the error when applying literature values, with mean absolute errors around 14 MPa and 15 MPa, respectively. The main difference when calibrating with only the gauge specimens compared to calibrating using the whole sample, is, as expected, larger scatter of the splintering/longitudinal shear type failure but a better estimate of the lower strength specimens, mainly the specimens with sloping shear type failures.

According to the failure criteria, the strength properties with the largest influence on the utilization ratio include tension strength parallel and perpendicular to the grain and the longitudinal shear strength. The model is relatively insensitive to the rolling shear strength values, and as such, the calibrated values may be extreme. The rolling shear was an unstable strength parameter when calibrating to the gauge specimens with Hashin criteria, and for predictions, the literature value was used in this case. It is also mentioned that the compression strength properties in Tsai-Wu may not be representative of the actual compression strengths since they are calibrated in absence of compression experimental data.

4.3 STRENGTH PREDICTION USING THE ANALYTICAL MODEL

To evaluate the numerical model's performance against a well-established analytical model, the generalized Hankinson's formula is considered. It defines off-axis tensile strength $f_{t,\alpha}$ as

$$f_{t,\alpha} = \frac{f_{t,0} f_{t,90}}{f_{t,0}\sin^n\alpha + f_{t,90}\cos^n\alpha} \tag{11}$$

where α is the angle between the load and the grain orientation, and n is a generalization parameter that is optimized by fitting the equation to the sample data, Generalization parameters within the range of 1.5 to 2.0 are typically regarded as suitable for predicting the (off-axis) tensile strength of wood [18].

The maximum 3D grain angle measured on the specimens are used in the formula. The strength properties and generalization parameter are calibrated to the data considering the whole sample and the gauge specimens. The calibrated parameters are given in Table 2. Figure 6 provides a comparison between the experimental and the predicted strengths, according to Hankinson's formula with strength properties calibrated to the whole data set.

The strength predictions of the analytical model are rather similar, in terms of error, when compared to the numerical model developed in this study. Indeed, compared to the analytical model, no significant improvement in the strength predictions was realized with the numerical model. An explanation to the similar results is given by analysis of the predicted failure locations. The location of failure is predicted for each specimen according to the most critical node. The critical node was frequently at the location of maximum 3D grain angle, which (due to the used interpolation method) is near the laser point measurements. In fact, the correlation coefficient between maximum 3D grain angle location and predicted failure location (for both failure criteria) was around 0.9. As such, both the numerical model and analytical model provide strength predictions largely based on the maximum measured 3D grain angle.

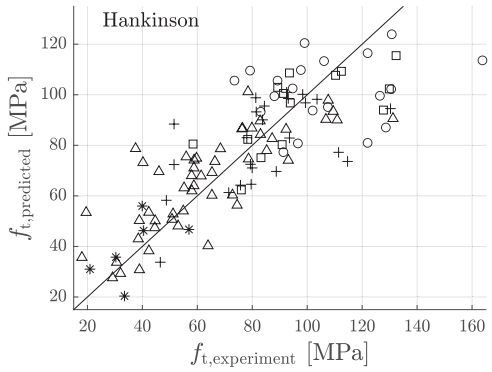

Figure 6: *Comparison between predicted and experimental strength for the Hankinson analytical model with strength properties and exponential parameter n calibrated to the whole sample.*

5 CONCLUSION AND OUTLOOK

In the present paper, a numerical model is developed for the prediction of tension strength of small-scale birch wood specimens with measured grain angles. The strength was predicted according to local stresses obtained from

https://doi.org/10.52202/069179-0058

the finite element model and two failure criteria, Hashin and Tsai-Wu, with a stress averaging approach. The model is compared to the experimental results and a simple analytical model. Results indicate:

- The maximum grain angle is a good indicator of strength. The predicted failure location of the model occurred around the location of the maximum measured 3D grain angles.
- The performance of the numerical model was limited by the information available of the test specimens. With grain angle being the driving indicator for strength, the maximum grain angle within the gauge region was the dominant factor in the strength predictions.

Potential future developments to the presented numerical model include the following:

- Associate the material properties (strength and stiffness) with various growth features identified on each specimen, such as growth ring width, distance to pith, or eigenfrequency. Use correlations between the growth features and the mechanical properties to estimate the material properties applied to the model and corresponding predictions.
- Include information about the location of the pith in the analysis. This way the material can be modelled with cylindrical orthotropy, i.e., tangential, and radial orientations can be defined, and orthotropic failure criteria can be used with related orthotropic strength properties.
- Increase the number of grain angle measurements (laser points) and measure also diving angles to better represent the grain flow of the specimen and the maximum grain angle.
- Consider the actual fracture process in the simulations. This can be implemented via damage or fracture mechanics-based formulations such as smeared crack models (local or non-local damage) or discrete crack models, e.g., cohesive cracks with extended finite element method.

REFERENCES

[1] P. Guindos and M. Guaita, "A three-dimensional wood material model to simulate the behavior of wood with any type of knot at the macro-scale," *Wood science and technology,* vol. 47, no. 3, pp. 585-599, 2013.

[2] M. Lukacevic, G. Kandler, M. Hu, A. Olsson and J. Füssl, "A 3D model for knots and related fiber deviations in sawn timber for prediction of mechanical properties of boards," *Materials & Design,* vol. 166, no. 107617, 2019.

[3] V. Kilde, K. H. Solli, B. Pitzner, P. Lind and J. Bramming, "Bjørk i synlige konstruksjoner (Birch in visible constructions). Rapport nr. 67.," Norsk Treteknisk Institutt, 2006.

[4] S. Collins and G. Fink, "Modeling the tensile mechanical properties of silver birch timber boards," *Construction and Building Materials,* vol. 344, no. 128147, 2022.

[5] S. Collins and G. Fink, "Grain angle determination of silver birch by laser light scattering and tensile fracturing," *Mater Struct,* vol. 55, no. 162, 2022.

[6] ISO 13061-6:2014(E), "Physical and mechanical properties of wood — test methods for small clear wood specimens — part 6: Determination of ultimate tensile stress parallel to grain," International Organization for Standardization, Geneva, 2014.

[7] S.-P. Simonaho, J. Palviainen, Y. Tolonen and R. Silvennoinen, "Determination of wood grain direction from laser light scattering pattern," *Optics and lasers in engineering,* vol. 41, no. 1, pp. 95-103, 2004.

[8] S. Collins, Mechanical behavior of silver birch structural timber under compression and tension loading, Aalto University doctoral thesis 175 Helsinki, 2022.

[9] J. M. Dinwoodie, Timber: its nature and behaviour, CRC Press London, 2000.

[10] Z. Hashin, "Failure criteria for Unidirectional Fiber Composites," *Journal of Applied Mechanics,* vol. 47, pp. 329-334, 1980.

[11] S. Tsai and E. Wu, "A General Theory of Strength for Anisotropic Materials," *Journal of Composite Materials,* vol. 5, pp. 58-80, 1971.

[12] P. Guindos, "Comparison of different failure approaches in knotty wood," *Drewno: prace naukowe, doniesienia, komunikaty,* vol. 57, 2014.

[13] P. J. Gustafsson, "Mean Stress Approach and Initial Crack Approach," in *Fracture mechanics models for strength analysis of timber beams with a hole or a notch - A Report of RILEM TC-133*, Lund, Lund University, Sweden, 2002.

[14] S. Thelandersson and H. J. Larsen, Timber Engineering, first ed, West Sussex: Wiley, 2003.

[15] R. Wagenführ and C. Scheiber, Holzatlas, Leipzig: Fachbuchverlag, 1974.

[16] S. Collins and G. Fink, "Mechanical behaviour of sawn timber of silver," *Wood Material Science & Engineering,* vol. 17, no. 2, pp. 121-128, 2022.

[17] T. Ehrhart and R. Brandner, "Rolling shear: Test configurations and properties of some European soft- and hardwood species," *Engineering Structures,* vol. 172, pp. 554-572, 2018.

[18] F. F. P. Kollmann and W. A. Cote, Principles of Wood Science, New York: Springer-Verlag, 1968.